HAL
open science

The buried caldera of Misti volcano, Peru, revealed by combining a self-potential survey with elliptic Fourier function analysis of topography

Anthony Tort, Anthony Finizola

To cite this version:

Anthony Tort, Anthony Finizola. The buried caldera of Misti volcano, Peru, revealed by combining a self-potential survey with elliptic Fourier function analysis of topography . Journal of Volcanology and Geothermal Research, 2005, 141, pp.283-297. 10.1016/j.jvolgeores.2004.11.005 . hal-01465828

HAL Id: hal-01465828

https://hal.science/hal-01465828v1

Submitted on 13 Feb 2017

HAL is a multi-disciplinary open access archive for the deposit and dissemination of scientific research documents, whether they are published or not. The documents may come from teaching and research institutions in France or abroad, or from public or private research centers.

L'archive ouverte pluridisciplinaire **HAL**, est destinée au dépôt et à la diffusion de documents scientifiques de niveau recherche, publiés ou non, émanant des établissements d'enseignement et de recherche français ou étrangers, des laboratoires publics ou privés.

The buried caldera of Misti volcano, Peru, revealed by combining a self-potential survey with elliptic Fourier function analysis of topography

Anthony Tort[a,*], Anthony Finizola[b]

[a]*Laboratoire Magmas et Volcans, Université Blaise Pascal et CNRS, OPGC, IRD, 5 rue Kessler, 63038 Clermont-Ferrand, France*
[b]*Istituto Nazionale di Geofisica e Vulcanologia, INGV-Sezione di Palermo, Via Ugo La Malfa 153, 90146 Palermo, Italy*

Abstract

This survey proposes a new approach to identify buried caldera boundaries of a volcanic cone, combining (1) a systematic elliptic Fourier functions (EFF) analysis on the contour lines based on the external shape of the edifice with (2) self-potential (SP) measurements on volcano flanks. The methodology of this approach is to investigate the relationships between (1) vertical morphological changes inferred from EFF analysis and (2) lateral lithological transition inside the edifice inferred from SP/ elevation gradients. The application of these methods on Misti volcano in southern Peru displays a very good correlation. The three main boun daries evidenced by hierarchical cluster analysis on the contour lines coincide with the two main boundaries characterised by SP signal and with a secondary SP signature related with a summit caldera. In order to explain these results showing a very good correlation between morphologic and lithologic changes as function of elevation, caldera boundaries have been suggested. The latter would be located at an average elevation of (1) 4350–4400 m, (2) 4950–5000 m, and (3) 5500– 5550 m.

For the lowest boundary in elevation, the coincidence with the lateral extension of the hydrothermal system inferred from SP measur ements suggests that caldera walls act as a barrier for lateral extension of hydrothermal systems. In the summit area, the highest boundary has been related with the summit caldera, inferred by a secondary SP minimum and geological evidence.

1. Introduction

The morphology of a volcanic cone is the first information accessible to volcanologists. It is linked to the eruptive activity and to the different constructive and destructive stages that built the volcanic edifice. A

* Corresponding author. 27, Route de Baugy, F-18800 Villabon, France. Tel.: +33 2 38 69 21 11.

E-mail addresses: anthony.tort@laposte.net (A. Tort), a.finizola@pa.ingv.it (A. Finizola).

specific morphological change can be associated to each kind of eruptive activity. Indeed, on the flanks of a volcanic cone, morphological changes can be subdivided in several groups: (1) progressive morphological changes as a function of elevation related to tephra-fall; (2) sharp or drastic lateral morphological changes associated with sector collapse, surge, lahar, debris flow, or lava flow; and (3) sharp or drastic morphological changes as a function of elevation related to caldera or summit crater formation. Therefore, according to the morphological analysis carried out, looking for vertical or lateral transitions, different related eruptive dynamism could be evidenced.

In volcanology, the recognition of the largest destructive events on a volcano, in particular, those associated with caldera formation, is a priority to assess the recurrence and the related hazard of this phenomenon. Therefore, the present survey is focused on the identification of caldera boundaries, looking for morphological changes as a function of elevation.

The first question was: "Is it possible to deduce parts of a volcano's history by a systematic mathematical analysis based on the morphology of the cone?" One of the possibilities is to quantify the morphology of the contour lines. This idea is not new (Garcia-Zuniga and Parrot, 1998), but a great number of morphometric methods to study a closed contour exist. These methods are very widespread in palaeontology and sedimentology, but their use in volcanology is quite new. Three methods are generally used to quantify a closed contour: the Bézier curves (which are not very often used), the Eigenshape analysis (Lohmann, 1983) and the Fourier analysis (Lestrel, 1997). Other methods also exist for quantifying morphology, such as Procrustes analysis or wavelet analysis. However, the latter are not adapted to our objectives: Procrustes analysis need landmarks, which are not present on a contour line, and wavelet analysis is more adapted for looking at the periodicity of a signal and is not suitable for compare different features. Fourier analysis was therefore used for this survey because it is quick and easy, and because it is well known (e.g., Christophers and Waters, 1974; Lestrel, 1997; Tort, 2003a, b). It also allows us to obtain data that are simple to treat using multivariate analyses.

Moreover, we investigated structural boundaries on the same volcanic cone using self-potential (SP) method. In a volcanic context, electrical potentials represent the ground surface electrical field signature of some polarisation mechanisms occurring in the soil. These SP signals are commonly thought to be created by electrokinetic coupling of fluid flow dragging the excess of charges located in the vicinity of the pore water/mineral interface. For silicates or aluminosilicate rocks, this electrical diffuse layer is generally positive and induces an excess of positive charges toward the flow direction (e.g., Ishido and Mizutani, 1981; Jouniaux et al., 2000; Pride, 1994; Revil et al., 1999a,b; Lorne et al., 1999a,b; Revil and Leroy, 2001; Guichet and Zuddas, 2003). Therefore, SP is frequently used on active volcanoes to identify through positive SP anomalies, fluid uprising associated with hydrothermal systems (e.g., Zablocki, 1976; Lénat et al., 1998; Malengreau et al., 1994; Finizola et al., 2002, 2003).

In the case of an active volcano with a classical hydrothermal system centred on the summit area, a general SP pattern subdividing its flanks in two zones is commonly observed: (1) in the lower part of the edifice, a zone with a negative SP/elevation gradient corresponds to the hydrogeological zone where meteoritic water flows down toward the aquifer (Aubert and Yéné Atangana, 1996; Darnet et al., 2003); and (2) in the upper part of the edifice, a zone with a positive SP/elevation gradient corresponds to the hydrothermal zone where fluids rise-up toward the surface (e.g., Sasai et al., 1990; Aubert and Dana, 1994; Hashimoto and Tanaka, 1995; Revil et al., 2003a,b).

One of the advantages of the SP signal is that it integrates numerous information coming from different depth and origin inside this large wavelength signal subdividing hydrothermal and hydrogeological zones (Finizola et al., 2003). In particular, several authors identified a linearity in the negative SP/elevation gradient in hydrogeological zone on shield volcanoes. The gradient has been related to the progressive increase in thickness of the unsaturated zone as confirmed by observations at boreholes and by electrical soundings carried out on Piton de la Fournaise volcano (Lénat, 1987; Boubekraoui et al., 1998), on Adagsdar volcano (Corwin and Hoover, 1979), or on Kilauea (Jackson and Kauahikaua,

1987). A change in slope of the self-potential/elevation gradient (Lénat, 1987; Jackson and Kauahikaua, 1987) can be attributed to a lateral change in permeability affecting the piezometric gradients along the slope of the volcano (Revil et al., 2002, 2003a,b).

On andesitic volcanoes, sharp break in slopes of these linear SP/elevation gradients encountered in hydrogeologic and hydrothermal zones have been interpreted as resistivity transitions responsible for the distortion of the electrical field propagating from the source toward the surface (e.g., on Usu volcano, Nishida and Tomiya, 1987, or on Hokkaido Komagatake volcano, Matsushima et al., 1990).

Other theoretical considerations could be attempted to explain these sharp transitions in the linear SP/elevation gradients. In particular, it could be considered that these transitions do not result from differences in the electrical field propagation or in the piezometric gradient, but in some changes in the electrical field generation. In this way, one or several parameters implicated in the SP source generation by electrokinetic processes and well known in the Helmholtz–Smoluchowski formula (e.g., Lorne et al., 1999a,b; Pengra et al., 1999) could be changed. In natural environments, it is important to note that all these parameters (the dielectric constant of the fluid, the viscosity of the fluid, the electric conductivity of the fluid, the pH of the fluid, the zeta potential, and the difference of pressure induced by the fluid flux) are directly linked (through mineralogy, permeability and porosity) or indirectly (through water–rock interaction) to the lithology (Revil et al., 1999a; Lorne et al., 1999a,b; Pride and Morgan, 1991). In other words, whatever the cause responsible of the sharp break in slope of the linear SP/elevation gradients, a lithological change must be invoked.

Therefore, our approach was to carry out SP radial profiles along the flanks of a volcanic edifice in order to observe transitions in the SP signal that could be related to lateral lithological transition. Such transitions can be generated by important destructive or constructive events that built the volcanic edifice. A caldera-forming event for instance, which has been mentioned above, could create such lithological boundaries between the older products of the external caldera flanks and the refilled material, but other changes in the rock petrology during the different stages which built the volcanic edifice can also be involved.

In order to discriminate the nature of the volcanic events responsible for the main vertical structuration of a volcanic cone and to identify in particular possible caldera boundaries, we therefore investigated the heterogeneity of a volcanic cone using the self-potential (SP) method and then we compared the results observed by the SP method with those obtained by the Fourier analysis on the contour lines.

Misti was chosen to apply the two above-mentioned techniques. This andesitic stratovolcano is located in southern Peru, 17 km from Arequipa, (~900,000 inhabitants), Peru's second largest city. Misti is one of the seven potentially active volcanoes of south Peru, which have erupted since the Spanish conquest (Bullard, 1962; de Silva and Francis, 1990). Misti, 5822 m a.s.l. (above sea level) rises 3.5 km above the city of Arequipa, posing a major threat to the population.

Misti lies within a complex tectonic setting. It is surrounded by the Altiplano, the tectonic depression of Arequipa and by the dormant Chachani volcano and the extinct Pichupichu volcano. The growth of Misti volcano has been divided in four stages by Thouret et al. (2001). Misti is a composite edifice comprising an eroded stratovolcano termed Misti 1, partially overlapped by two stratocones termed Misti 2 and 3, and a summit cone Misti 4. Misti 1 (833 to 112 k.y.) essentially consists of lava flows and debris avalanche deposits. Misti 2 (112 to 40 k.y.) is characterised by lava flows and dome-collapse deposits. At the end of stage 2, ca. 50 to 40 k.y., the eruption of nonwelded ignimbrites of 3–5 km^3 in volume is probably associated with the formation of an incremental caldera. Misti 3 stage (40 to 11 k.y.) is mainly built up of lava flows, block-and-ash, and ash-flow deposits. Misti 3 also ended with the formation of a summit caldera to which pyroclastic flows and fall deposits were linked. From 11 k.y. to the present, Misti 4 stage corresponds to the growth of the summit cinder cone and to the formation of two summit craters. Pyroclastic flow, fall, and debris avalanche deposits are associated with this eruptive stage (Thouret et al., 2001). At the present time, the smaller of the two summit craters, 550 m in diameter and 200 m deep, contains a 130-m-wide and 15-m-high andesitic plug.

2. Methods

2.1. Self-potential

During field campaigns in 1997 and 1998, a total of 167 km of SP profiles with 100 m spacings were carried out on Misti volcano (Finizola et al., 2004). Data were collected along 10 radial profiles extending from the summit (5822 m a.s.l.) to the lower flanks of the edifice (~3000 m a.s.l.; Fig. 1). Two concentric profiles, located in the summit area and at the base of the lower flanks of the edifice, were carried out to ensure the closure of the radial profiles. A closure correction (less than 20 mV for three profiles, as much as 50 mV for five profiles and as much as 100 mV for two profiles) was calculated and distributed linearly on the profiles.

The SP equipment consists of a high-impedance voltmeter, a pair of $Cu/CuSO_4$ non-polarising electrodes, and an insulated Cu cable 300 meters long. During the fieldwork, the electrical contact between the electrode and the soil was tested before every SP measurement, by measuring the resistance of the circuit. SP stations were geo-referenced using a portable GPS navigation receiver. The elevation of each station was therefore extracted from a precise digital elevation model of the volcano. In order to find structural discontinuities, each radial profile was analysed as a function of elevation.

2.2. Elliptic Fourier functions

Two methods of Fourier analysis exist: "classical" Fourier series and elliptic Fourier functions (EFF). "Classical" Fourier series use the radius from the barycentre of the shape studied. However, as some vectors stemming from the barycentre cut the contour line studied twice, the EFF method was, therefore, chosen for study based on the detailed analysis along the contour lines. In order to perform the Fourier analysis, 512 points equally spaced along the length of the contour lines are selected on each one.

The EFF method (Kuhl and Giardina, 1982) allows a Fourier series development where the abscissa and ordinate of each point are expressed as a function of the curvilinear abscissa of that point (Fig. 2). This allows a parametric formulation where the functions $x(t)$ (for the x-axis) and $y(t)$ (for the y-axis) can be obtained and expanded into two Fourier series:

$$x(t) = a_0 + \sum_{j=1}^{k} \left[a_j \cos\left(\frac{2j\pi t}{T}\right) + b_j \sin\left(\frac{2j\pi t}{T}\right) \right], \tag{1}$$

and

$$y(t) = c_0 + \sum_{j=1}^{k} \left[c_j \cos\left(\frac{2j\pi t}{T}\right) + d_j \sin\left(\frac{2j\pi t}{T}\right) \right], \tag{2}$$

where k is the number of harmonics used, j is the order of the harmonic, and T is the outline perimeter.

The terms a_j, b_j, c_j, and d_j are the Fourier coefficients of the harmonic j and are calculated as follows (Kuhl and Giardina, 1982):

$$a_j = \frac{1}{2j^2\pi^2} \sum_{i=1}^{n} \frac{\Delta x_i}{\Delta t_i} \left[\cos\left(\frac{2j\pi t_i}{T}\right) - \cos\left(\frac{2j\pi t_{i-1}}{T}\right) \right], \tag{3}$$

$$b_j = \frac{1}{2j^2\pi^2} \sum_{i=1}^{n} \frac{\Delta x_i}{\Delta t_i} \left[\sin\left(\frac{2j\pi t_i}{T}\right) - \sin\left(\frac{2j\pi t_{i-1}}{T}\right) \right], \tag{4}$$

$$c_j = \frac{1}{2j^2\pi^2} \sum_{i=1}^{n} \frac{\Delta y_i}{\Delta t_i} \left[\cos\left(\frac{2j\pi t_i}{T}\right) - \cos\left(\frac{2j\pi t_{i-1}}{T}\right) \right] \tag{5}$$

and

$$d_j = \frac{1}{2j^2\pi^2} \sum_{i=1}^{n} \frac{\Delta y_i}{\Delta t_i} \left[\sin\left(\frac{2j\pi t_i}{T}\right) - \sin\left(\frac{2j\pi t_{i-1}}{T}\right) \right]. \tag{6}$$

Terms a_0 and c_0 are constants and computed as follows:

$$a_0 = \frac{1}{T} \sum_{i=n}^{n} \frac{1}{2} \frac{\Delta x_i}{\Delta t_i} \left(t_i^2 - t_{i-1}^2 \right) - \frac{\Delta x_i}{\Delta t_i} t_i, \tag{7}$$

and

$$c_0 = \frac{1}{T} \sum_{i=n}^{n} \frac{1}{2} \frac{\Delta y_i}{\Delta t_i} \left(t_i^2 - t_{i-1}^2 \right) - \frac{\Delta y_i}{\Delta t_i} t_i, \tag{8}$$

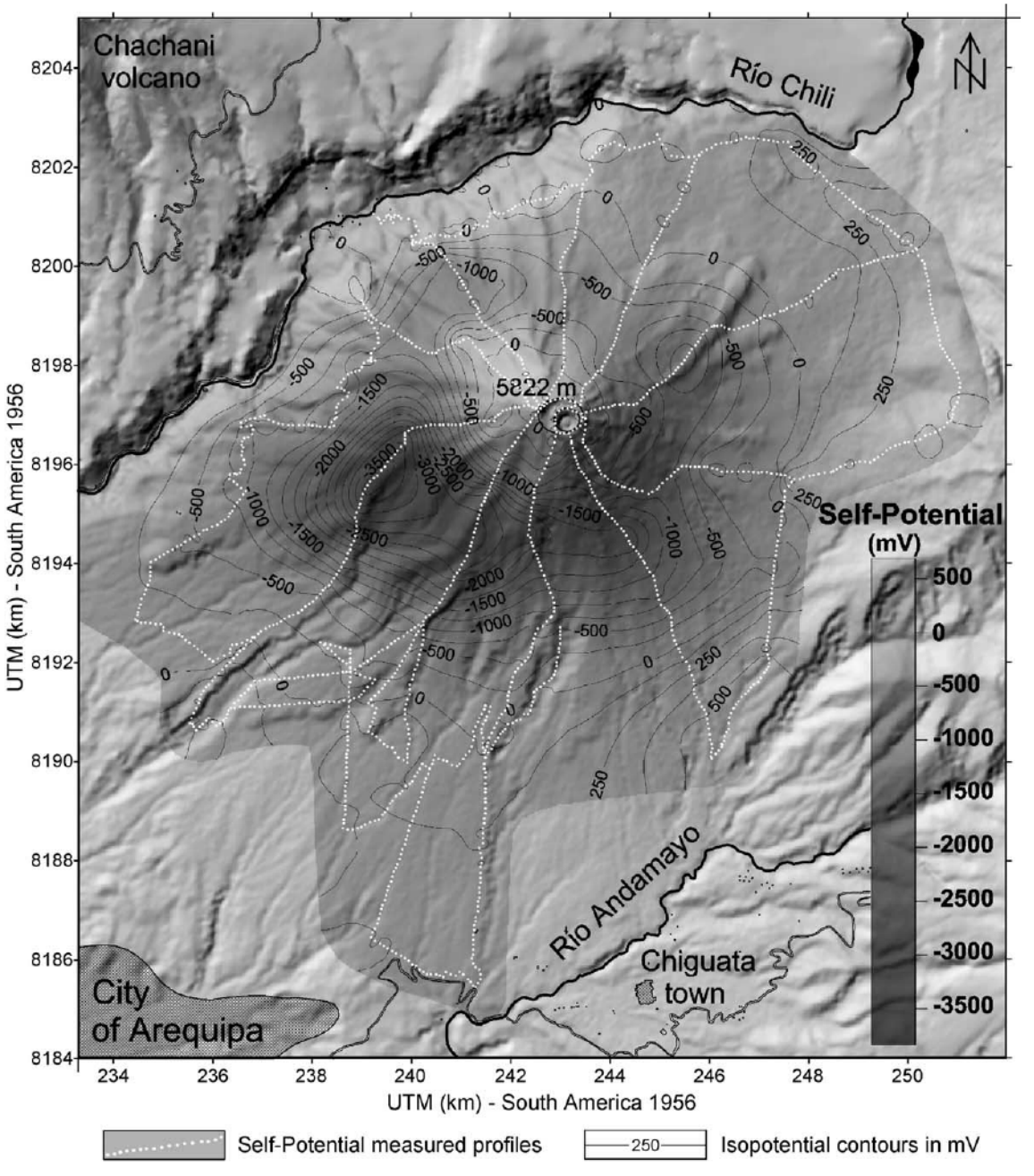

Fig. 1. SP map of Misti volcano superimposed on a shaded relief map showing volcano-structural features. (Digital elevation model improved by SAR-interferometry, courtesy of Jean-Luc Froger).

where T is the outline perimeter; x_i is the modulus of the projection onto the x-axis of the segment between points i and i+1 of the outline (Fig. 2); y_i is the modulus of the projection onto the y-axis of the segment between points i and i+1 of the outline (Fig. 2); Δt_i is the modulus of the segment between

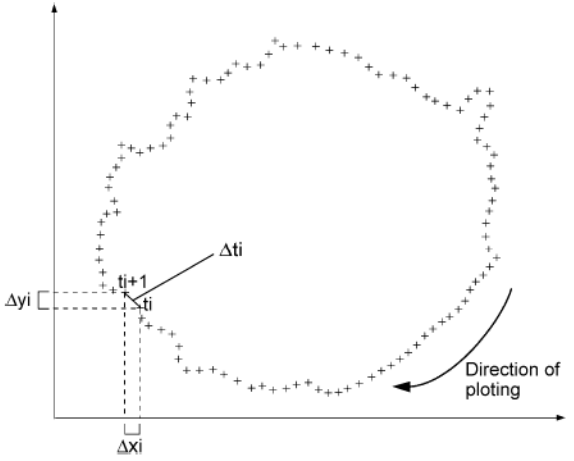

Fig. 2. Illustration of the parameters used for calculating the Fourier coefficients of an elliptical Fourier function on the contour line 4200 m of Misti volcano; for better clarity, only a part of the 512 original points, equally spaced, is plotted. The contour line is subdivided by dots in 512 segments of equal length so Δt_i is constant between two points. Δx_i is the difference between the abscissa of point t_i and the abscissa of point t_{i+1}, and Δy_i is the difference between the ordinate of point t_i and the ordinate of point t_{i+1} (from Viguier and Tort, 2000 modified).

points i and i+1 of the outline (Fig. 2); t_i is the curvilinear abscissa of the index point i; and n is the number of points on the outline.

The amplitude of a harmonic is calculated as follows:

$$amp_j = \frac{1}{2}\sqrt{a_j^2 + b_j^2 + c_j^2 + d_j^2} \tag{9}$$

High-amplitude (i.e., those with large magnitude) harmonics describe the main outline characteristics. These are generally the low-order harmonics. In contrast, low-amplitude harmonics (with small magnitudes) characterise the details; these are usually the high-order harmonics.

The elliptic Fourier functions are of great interest because they are reversible. It is possible to reconstitute the shape from the harmonic's coefficients. The greater the number of harmonics added, the better the reconstruction of the shape (Fig. 3). For example, the analysis of the contour line 4200 m shows that the concordance between the original contour line and the reconstructed contour line using the coefficients of the five first harmonics is 97.23%. The concordance between the original contour line and the reconstructed contour line using 30 harmonics is 99.37%.

The Fourier analysis was done using the software "Four ellipse" (Schaaf et al., 1999). The contour lines analysed on Misti are equally spaced at 50 m. The lowest contour line is 4050 m and the highest is 5650 m. The first 30 harmonics were used to characterise each contour line, which allowed for each one of them a concordance between the original line and the reconstructed one to be greater than 99%. In order to find discontinuities in the succession of the contour lines, the coefficients of the first thirty harmonics or the amplitude of the harmonic can be analysed using hierarchical cluster analysis. Calculation of a harmonic amplitude involves the four coefficients of the harmonic (see Eq. (9)). This implies that two contour lines having different Fourier coefficients may display the same amplitude. Therefore, due to the loss of information characterizing the amplitude, hierarchical cluster analyses was performed on the coefficients (Tort, 2003b).

3. Results

3.1. SP analysis

The analysis of SP profiles as a function of elevation (Fig. 4) revealed a typical "V" shape signal dividing (1) a negative SP/elevation gradient related to the hydrogeological zone in the lower part of the edifice from (2) a positive SP/elevation gradient related to the hydrothermal zone in the upper part of the edifice. Moreover, (3) in the highest part of the edifice, a plateau zone characterises the SP signal. These three main subdivisions of the SP signal (Fig. 4) can be also subdivided into several linear segments separated by sharp break in slopes. For each segment, the SP/elevation gradient, called correlation coefficient "Ce" in mV/m (by Jackson and Kauahikaua, 1987), have been calculated. Based on these Ce values, different zones have been defined along each profile. In the hydrogeological zone, four subdivisions have been identified (Fig. 4); they are called Hz1, Hz2, Hz3, and Tz (Hz and Tz standing for, respectively, Hydrogeological zone and Transitional zone). Increasing the elevation, an increase of Ce in absolute value characterises the sectors Hz1 to Hz3 ($|Ce|_{(Hz1)}<|Ce|_{(Hz2)}<|Ce|_{(Hz3)}$), and close to the SP minimum, $Ce_{(Tz)}$ displays a drastic diminution in

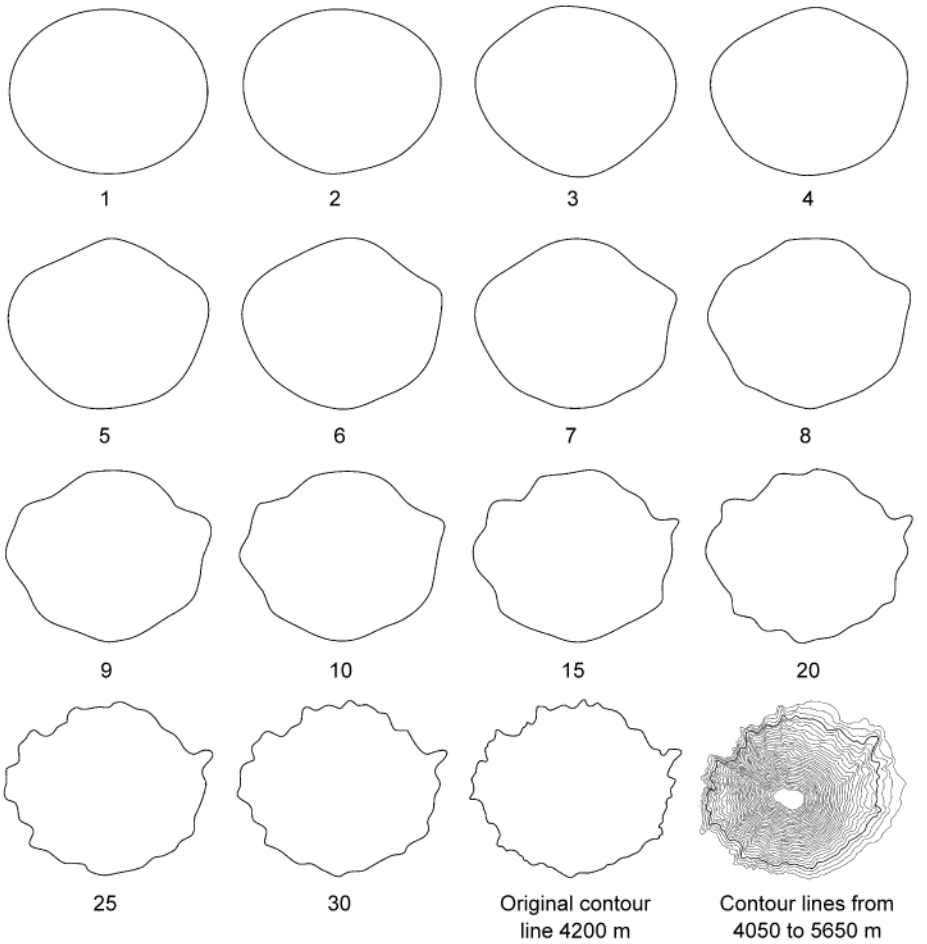

Fig. 3. Comparison between the shape of the original 4200 m contour line of Misti volcano and the contour lines 4200 m reconstructed from EFF method using the addition of 1, 2, 3, 4, 5, 6, 7, 8, 9, 10, 15, 20, 25, and 30 harmonics. The analysis of all the contours lines (from 4050 to 5650 m) of this survey have been performed using 30 harmonics corresponding to a concordance with the original contour line higher than 99%. The drawing in the lower right corner correspond to all the original contour lines analysed in this study.

absolute value of the SP/elevation gradient. Similarly, in the hydrothermal system, four distinct zones called LCz1, LCz2, LCz3, and UCz (LCz and UCz standing for, respectively, Lower Convective zone and Upper Convective zone), were defined (Fig. 4), where $Ce_{(LCz1)}<Ce_{(LCz2)}>Ce_{(LCz3)}$. In the UCz zone, the linearity in the SP/elevation relationship is not so clearly defined but the average gradient decreases drastically compared to the $Ce_{(LCz3)}$ value. This zone is also characterised by a SP minimum of several hundreds of mV in amplitude and several hundreds of meters of wavelength (Fig. 4). The distribution on a map of these distinct zones defined along the 10 radial profiles allows to obtain the shape of these transitions at the scale of the volcano (Fig. 5). These latter display concentric shapes mostly centred on the present-day summit craters. The elevation of the lower boundary of each zone has been extracted along each profile and an average elevation was calculated for each zone. The results display the following subdivisions: (1) ~3660 m for Hz2; (2) ~3960 m for Hz3; (3) ~4090 m for Tz; (4) ~4400 m for LCz1; (5) ~4520 m for LCz2; (6) ~4710 m for LCz3; (7) ~4970 m for UCz; and (8) ~5410 m for SP secondary minimum. Obviously, these limits are not located at a constant elevation all around the

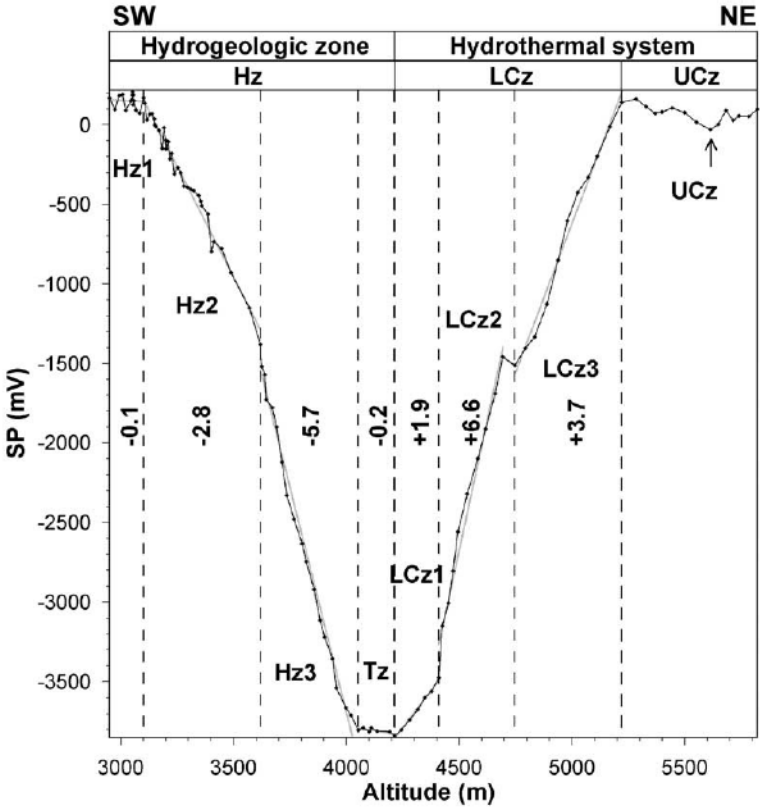

Fig. 4. Example of SP profile number 2 as a function of elevation showing how the distinct zones based on SP/elevation gradient were determined. Numbers represent the slope value of each linear SP/elevation segment (expressed in mV/m).

edifice, but the average value gives a good information on the average altitude where this transition occurs.

3.2. The elliptical Fourier function analysis

A hierarchical cluster analysis was performed on the coefficients of the first thirty harmonics. Distances between the groups are measured using the Euclidian distance. The aggregation rule used is the UPGMA (unweighted pair-group method using arithmetic averages).

No statistical test exists that can put a limit in trees obtained using a hierarchical cluster analysis (Shi, 1993). In this study, the limit chosen for Misti volcano allows the identification of three limits (Fig. 6):

(1) the best defined limit, between the contour lines 4950 and 5000 m,
(2) the second limit, between the contour lines 5500 and 5550 m, and
(3) the third limit, between the contour lines 4350 and 4400 m.

3.3. Comparison between the elliptical Fourier function analysis and the SP results

As discussed in the Introduction, Ce transitions are related to geological transitions: the positive anomaly of about 6-km large can be interpreted as a signature of polarization mechanisms occurring at depth, and variations of Ce as disruptions of this electrical signal induced by shallower geological boundaries. Moreover, due to the sharp transition of the SP/elevation gradient at the scale of the sampling rate (100 m), this suggests that the geological boundaries responsible for the different Ce zones are shallow (<100 m). In the case of a caldera-forming event, we should therefore

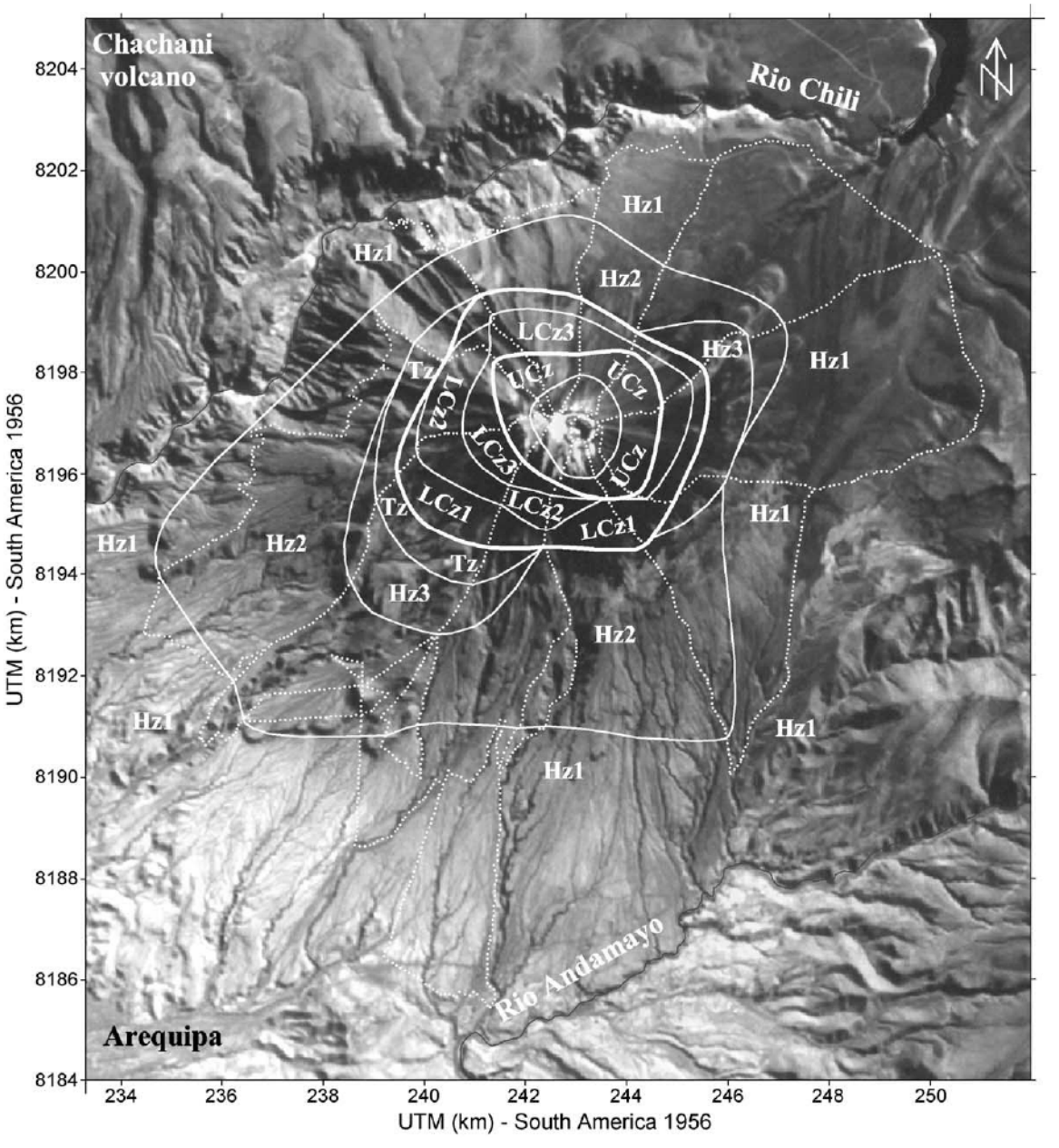

Fig. 5. Ce limits on Misti volcano defined along SP profiles (Fig. 4) superimposed on a Landsat image. Dashed line represents SP minimum in the summit area defined along the SP profiles (Fig. 4). Hz, Tz, LCz and UCz stand for 'Hydrogeological zone', 'Transition zone', 'Lower Convective zone,' and 'Upper Convective zone', respectively.

expect that, due to its shallow depth, this transition should be also evidenced in the volcanic morphology of the cone by the hierarchical cluster analysis of the contour lines. Hence, a comparison between the average elevation of the Ce transition and the limit obtained by the hierarchical cluster analysis of the contour lines was carried out (Fig. 7). The result of the correlation of these two distinct approaches, visual-

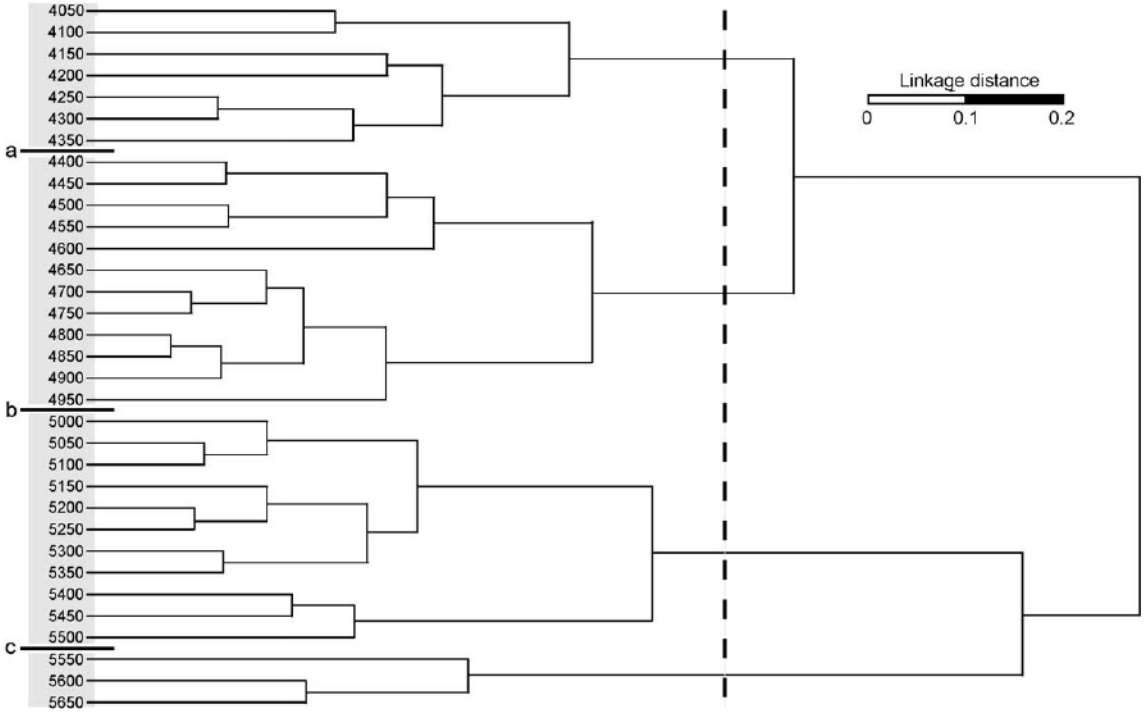

Fig. 6. Hierarchical cluster analysis of the contour lines of Misti volcano (equidistance at 50 m) performed on the coefficients of the first thirty harmonics. The vertical dashed line corresponds to the limit chosen for defining three main horizontal limits: a, b, and c. Pale grey colour allows a better identification of the four groups of contours lines separated by a, b, and c limits. These three limits a, b, and c are discussed in the text.

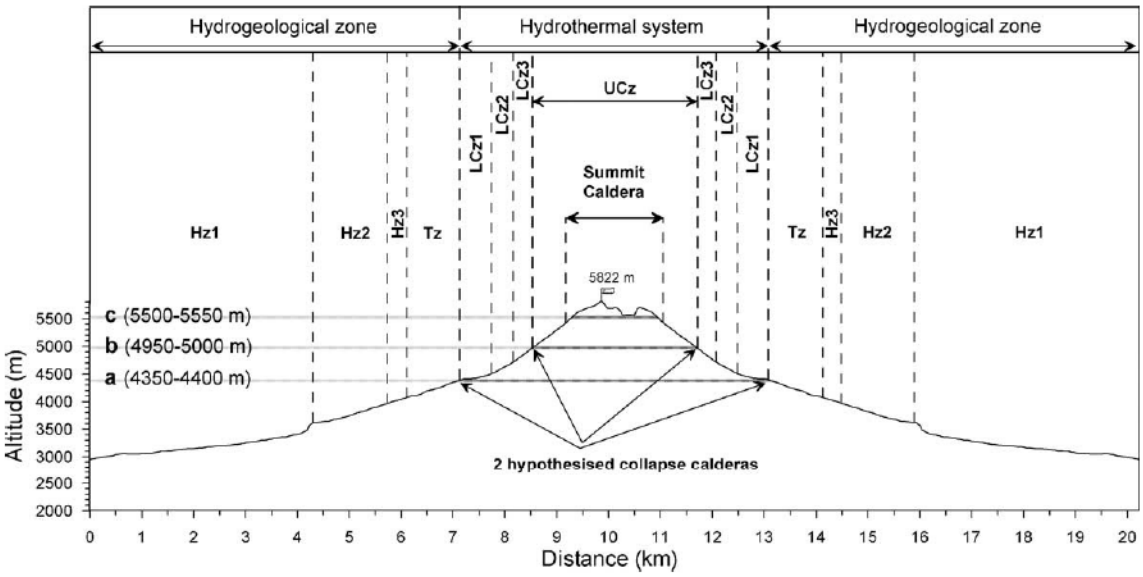

Fig. 7. Cross-section of Misti volcano showing the correlation between the boundaries identified by hierarchical cluster analysis and the average elevation of the transitions inferred by Ce transitions.

ised along a topographic cross-section of the volcano, displays that the three limits encountered from the hierarchical cluster analysis of the contour lines seem to coincide with boundaries identified by observed Ce transitions:

(1) The first transition at lowest altitude, between 4350 and 4400 m, corresponds to the limit between hydrogeologic and hydrothermal systems (beginning of LCz1, in Fig. 7). This limit has been proposed as a possible boundary of a 6×5 km diameter incremental collapse caldera (Fig. 5) separating Misti 2 from Misti 3 edification stages, formed 40–50 ka ago (Thouret et al., 2001).
(2) Increasing in altitude, the second transition, located between 4950 and 5000 m, coincides with an important break in slope in the SP/elevation gradient, which corresponds to the limit between Lower and Upper Convective Zones and 4×3 km in diameter (Figs. 5 and 7). It is also possible to speculate the existence of a caldera boundary at this elevation, but there is a lack of geologic evidence to ensure this hypothesis.
(3) Finally, although a small shift of several tens of meters exists, the highest limit in elevation, located between 5500 and 5550 m could be related to the SP minimum located in the summit area in the Upper Convective zone, and 2×1.5 km in diameter (Figs. 5 and 7). This SP limit coincides with the boundary of the summit caldera indicated by geological evidence and formed 14–11 k.y. ago (Thouret et al., 2001).

4. Discussion

It is interesting to note that Fourier analysis applied to the contour lines of a volcanic cone can reveal morphological limits. These limits are linked to geological events that built the volcanic edifice. One of the outstanding results obtained by combining these mathematical and geoelectrical approaches is that, among the three main limits defined by the hierarchical cluster analysis, two of these also correspond to the two main subdivisions evidenced by the observed Ce transitions (Fig. 7). Based on these results, three questions are interesting to discuss: (1) how a geological limit can be identified at an elevation within a range precision of 50 m, when no geological boundary is defined in a such tight range of elevation; (2) what is the significance in terms of geological boundaries of the evidenced limits proven by this new combined approach; and (3) what are the limits in applying this new methodology on other volcanoes.

4.1. Precision in elevation range to determine geological boundaries

As discussed in the Introduction, sharp vertical changes in the morphology of a volcanic cone could be attributed to eruptive dynamism, such as caldera-forming event. According to this survey carried out on Misti volcano, these morphological changes are associated with changes in the inner part of the volcanic edifice. This good correlation between the hierarchical cluster analysis and Ce transitions strongly supports the hypothesis that these morphological changes can be related to circular structural boundaries, such as caldera walls.

However, it could appear not rigorous to determine a caldera boundary in a range of 50 m in elevation where no caldera boundary is constrained in such a tight range. Therefore, that means that our analysis could be a pure mathematical application with no consistence in term of geological limits. Hence, in order to ensure the consistence of the results encountered and the reality of the three identified boundaries, another hierarchical cluster analysis was carried out with a higher spacing between the contour lines. Similar results were found using a 100-m spacing between the contour lines, which allows the possible fluctuations in the elevation of caldera walls to be better taken into account (Fig. 8). The three limits are respectively located between 4350–4450, 4950–5050, and 5450–5550 m, which are the same but larger intervals than those encountered previously.

Therefore, although the geological boundaries can fluctuate in elevation more than the interval chosen for the contour line analysis, the transition can also be found. The latter will correspond to the average altitude, where the morphological transition is the more significant. In the same way, for Ce analysis, the comparison between our two approaches have been possible only because we have a cover in SP measurements of the entire volcanic cone (10 radial profiles),

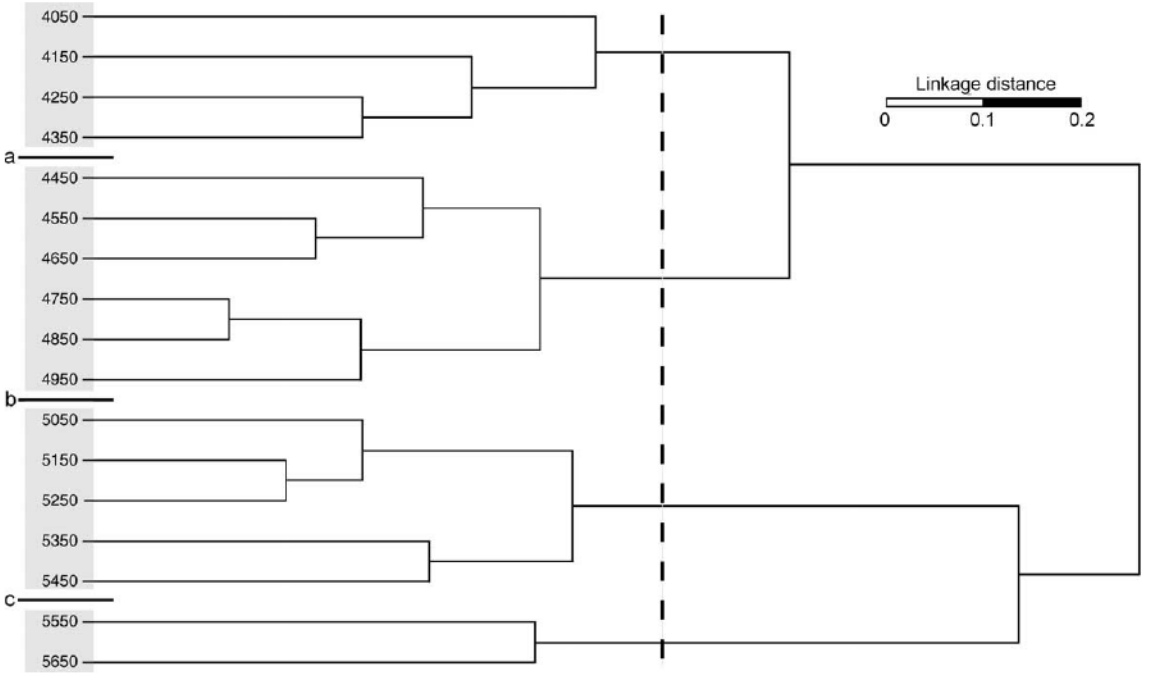

Fig. 8. Hierarchical cluster analysis of the contour lines of Misti volcano (equidistance at 100 m) performed on the coefficients of the first thirty. The vertical dashed line corresponds to the limit chosen for defining three main horizontal limits: a, b, and c. Pale grey colour allows a better identification of the four groups of contours lines separated by a, b, and c limits. These three limits a, b, and c are discussed in the text.

which allows us to determine a good average elevation where the transitions occurred. Among the three boundaries identified, the two largest boundaries were characterised by a very good correlation between morphological analysis and Ce transitions (see Fig. 7). Only a little shift was obtained in the summit area, probably due to the averaging carried out.

4.2. Geological signification of the identified boundaries

On Misti volcano, this pluridisciplinary survey allows the identification of three important boundaries in the volcanic cone. The lowest boundary in elevation evidenced between 4350 and 4400 m and speculated to be a caldera boundary also coincides with the hydrothermal system extent identified by the change of sign in Ce. This result suggests a correlation between caldera boundaries and lateral extension of hydrothermal fluid circulation. Such a correlation has been already observed on other volcanoes where geological boundaries were compared to SP surveys (e.g., on Karthala volcano, Lénat et al., 1998; on Stromboli volcano, Finizola et al., 2002). Furthermore, these surveys also display that caldera boundaries are sometimes associated with short wavelength SP anomalies (<100 m), suggesting a preferential fluid circulation along these structural boundaries. This means that faults associated with caldera borders appear as higher permeability planes that preferentially drain fluids. In the case of Misti volcano, a same pattern of higher permeability distribution along the caldera boundaries could explain the correlation between morphological changes and extent of the hydrothermal system. Indeed, the presence of a higher vertical permeability plane does not favour the lateral extent of fluids but rather its vertical circulation.

The two other limits evidenced in this survey are located inside the hydrothermal system. For the boundary located between 4950 and 5000 m, the associated drastic change in the SP gradient could be related to a distortion in the electrical field due to a difference in electrical resistivity, as proposed for Usu volcano (Nishida and Tomiya, 1987) or for Hokkaido Komaga-take volcano (Matsushima et al., 1990), and/or to a change in rock permeability inducing a change

in the piezometric gradient. In case of a caldera hypothesis, such a sharp difference in electrical resistivity and/or permeability could be related to the difference between the external products of the caldera and the refilled material.

For the summit caldera boundary, the associated SP minimum could be explained in the same way as the lowest boundary. Indeed, the coincidence between the SP minimum and the caldera boundary could be justified considering a preferential water infiltration along the structural boundary of the caldera wall.

Lithological boundaries built during constructive events of the cone (such as block-lava flow, tephra fall, pyroclastic flow, etc.) can be hypothesized as causing the five other Ce transitions (Hz2, Hz3, Tz, LCz2, LCz3 in (Figs. 4, 5, and 7)) observed through SP measurements, but with no clear equivalent in the morphological contour line analysis. Indeed, the two lowest boundaries in altitude (Hz2 and Hz3 in Fig. 5) have been related to the front of block-lava flows (Finizola et al., 2004), so lithological boundaries generated by constructive events are not able to induce significant vertical topographic transition.

4.3. Limitation of this new methodology for other volcanoes

On the basis or our results obtained on Misti, it would appear to be interesting to apply this quite cheap methodology to other volcanoes in the world. However, it is important to note that the good results obtained on Misti volcano can be attributed to several factors characterizing this particular volcanic edifice: (1) No eccentric structure of the volcano (e.g., adventitious craters) disrupting the EFF analysis, (2) the height of the edifice allows a closed contour line analysis on a huge range of elevation (from 4050 to 5650 m), (3) no adjacent volcano or pronounced topography on the basement of Misti, which allows us to analyze contour lines influenced only by the volcanic edifice, and (4) structural boundaries nearly centred on the present-day topography, allowing good assessment of the average elevation of the structural boundaries from the EEF analysis of the contours lines. Finally, the good correlation between the EFF analysis and the "Ce" transitions (Fig. 7) can be attributed to the huge amount of SP data (10 radial profiles), allowing the calculation of the average elevation of each transition with good accuracy.

5. Conclusions

According to this survey carried out on Misti volcano, Fourier analysis applied on contour lines appears to be an efficient tool to investigate the morphology of a volcanic cone. This method allows the identification of vertical limits subdividing the volcanic edifice.

The comparison between this mathematical approach (based on the external shape of the edifice) and a SP/elevation gradient analysis (based on the generation and the electrical field propagation inside the edifice) leads to the same subdivision of the cone.

These results support the geological importance of these boundaries. The latter could be linked to the largest destructive events involved in the formation of a volcanic cone, such as caldera-forming event, creating a huge vertical transition inside the volcanic cone, both in terms of drastic morphological and lithological transition.

This combined approach on Misti volcano pointed out three main structural limits that can be linked to caldera boundaries identified in previous geological surveys (Thouret et al., 2001) at: (1) 4350–4400 m (probably formed 50–40 ka ago), (2) 4950–5000 m but with no geological evidence, and (3) 5500–5550 m (probably formed 14–11 ka ago).

For the lowest boundary in elevation, the good correlation between the limit of the hydrothermal system and the boundary defined using elliptic Fourier function analysis suggests that caldera boundaries can constrain the lateral extension of hydrothermal systems.

Elliptic Fourier functions analysis and SP methods appear to be complementary methods to understand the formation of a volcanic cone. As a first approach, EFF would be useful for the study of volcanoes where calderas affect the whole cone. EFF would probably not be efficient with volcanic cones where eccentric structures affect the flanks of the cone or where the caldera boundary is to much decentred from the present-day topography. However, only the application of EFF on different volcanoes will specify the

application limits of this new method in volcanology. In particular, the combined approach with other geophysical methods able to define caldera boundaries such as gravimetry, SP, or high-resolution electrical resistivity tomography could be very promising.

Acknowledgements

The fieldwork in Self-Potential on Misti volcano (Finizola et al., 2004) was supported by the Institut de Recherche pour le Développement (IRD) and the Instituto Geofísico del Perú (IGP). The authors thank Laurence Jouniaux and an anonymous reader for the interesting reviews that have helped to improve the manuscript, and also Eric P. Verrecchia for correcting the English. A. F. acknowledges Jean-Luc Froger for providing the digital elevation model of Misti volcano improved by SAR-interferometry and Benjamin Van Wyk de Vries for the Landsat image of the Misti area.

References

Aubert, M., Dana, I., 1994. Interprétation of the self-potential radial profiles in volcanology: possibilities of the SP method for the monitoring of the active volcanoes. Bull. Soc. Geol. Fr., 113–122.

Aubert, M., Yéné Atangana, Q., 1996. Self-potential method in hydrogeological exploration of volcanic areas. Ground Water 34 (6), 1010–1016.

Boubekraoui, S., Courteaud, M., Aubert, M., Albouy, Y., Coudray, J., 1998. New insights into the hydrogeology of a basaltic shield volcano from a comparison between self-potential and electromagnetic data: Piton de la Fournaise, Indian ocean. J. Appl. Geophys. 40, 165–177.

Bullard, F.M., 1962. Volcanoes of Southern Peru. Bull. Volcanol. 24, 443–453.

Christophers, R.A., Waters, J.A., 1974. Fourier series as a quantitative descriptor of a miospore shape. J. Paleontol. 48 (4), 697–709.

Corwin, R.F., Hoover, D.B., 1979. The self-potential method in geothermal exploration. Geophysics 44 (2), 226–245.

Darnet, M., Marquis, G., Sailhac, P., 2003. Estimating aquifer hydraulic properties from the inversion of surface streaming potential (SP) anomalies. Geophys. Res. Lett. 30, 1679.

de Silva, S.L., Francis, P.W., 1990. Active and potentially active volcanoes of southern Peru: observations using Landsat thematic mapper and space shuttle imagery. Bull. Volcanol. 52, 286–301.

Finizola, A., Sortino, F., Lénat, J.-F., Valenza, M., 2002. Fluid circulation at Stromboli volcano, (Aeolian Islands, Italy) from self-potential and soil gas surveys. J. Volcanol. Geotherm. Res. 116 (1–2), 1–18.

Finizola, A., Sortino, F., Lénat, J.-F., Aubert, M., Ripepe, M., Valenza, M., 2003. The summit hydrothermal system of Stromboli: new insights from self-potential, temperature, CO_2 and fumarolic fluids measurements, with structural and monitoring implications. Bull. Volcanol. 65, 486–504.

Finizola, A., Lénat, J.-F., Macedo, O., Ramos, D., Thouret, J.C., Sortino, F., 2004. Fluid circulation and structural discontinuities inside Misti volcano (Peru) inferred from self-potential measurements. J. Volcanol. Geotherm. Res. 135, 343–360.

Garcia-Zuniga, F., Parrot, J.F., 1998. Analyse tomomorphométrique d'un édifice volcanique récent: Misti (Pérou). C. R. Acad. Sci. Paris, t. Sér IIa 327, 457–462.

Guichet, X., Zuddas, P., 2003. Effect of secondary minerals on electrokinetic phenomena during water–rock interaction. Geophys. Res. Lett. 30, 1714.

Hashimoto, T., Tanaka, Y., 1995. A large self-potential anomaly on Unzen volcano, Shimabara peninsula, Kuyshu island, Japan. Geophys. Res. Lett. 22 (3), 191–194.

Ishido, T., Mizutani, H., 1981. Experimental and theoretical basis of electrokinetic phenomena in rock–water systems and its applications to geophysics. J. Geophys. Res. 86, 1763–1775.

Jackson, D.B., Kauahikaua, J., 1987. Regional self-potential anomalies at Kilauea volcano. "Volcanism in Hawaii" chapter 40. USGS. Prof. Pap. 1350, 947–959.

Jouniaux, L., Bernard, M.L., Zamora, M., Pozzi, J.P., 2000. Streaming potential in volcanic rocks from Mount Pelée. J. Geophys. Res. 105 (4), 8391–8401.

Kuhl, F.F., Giardina, C.R., 1982. Elliptic Fourier features of a closed contour. Comput. Graph. Image Process. 18, 236–258.

Lénat, J.F., 1987. Structure and dynamique interne d'un volcan basaltique intraplaque océanique : Le Piton de la Fournaise (île de la Réunion). Thèse de doctorat ès sciences, Univ. Blaise Pascal, Clermont-Ferrand (France).

Lénat, J.F., Robineau, B., Durand, S., Bachélery, P., 1998. A self-potential survey of the summit zone of Karthala volcano (Grande Comore). C. R. Acad. Sci. 327, 781–788.

Lestrel, P. (Ed.), 1997. Fourier Descriptors and their Application in Biology. Cambridge University Press, Cambridge 466 pp.

Lohmann, G.P., 1983. Eigenshape analysis of microfossils: a general morphometric procedure for describing changes in shape. Math. Geol. 15 (6), 659–672.

Lorne, B., Perrier, F., Avouac, J.P., 1999a. Streaming potential measurements: 1. Properties of the electrical double layer from crushed rock samples. J. Geophys. Res. 104 (17), 17857–17877.

Lorne, B., Perrier, F., Avouac, J.P., 1999b. Streaming potential measurements: 2. Relationship between electrical and hydraulic flow patterns from rock samples during deformation. J. Geophys. Res. 104, 17879–17896.

Malengreau, B., Lénat, J.F., Bonneville, A., 1994. Cartographie et surveillance temporelle des anomalies de Polarisation Spontanée (PS) sur le Piton de la Fournaise. Bull. Soc. Géol. Fr. 165 (3), 221–232.

Matsushima, N., Michiwaki, M., Okazaki, N., Ichikawa, N., Takagi, A., Nishida, Y., Mori, H.Y., 1990. Self-potential study in

volcanic areas-Usu, Hokkaido Komaga-take and Me-akan. J. Fac. Sci., Hakkaido Univ., Ser. VII, Geophysics 8 (5), 465–477.

Nishida, Y., Tomiya, H., 1987. Self-potential studies in volcanic areas—Usu volcano. J. Fac. Sci., Hokkaido Univ., Ser. VII, Geophysics 8 (2), 173–190.

Pengra, D.B., Li, S.X., Wong, P.-Z., 1999. Determination of rock properties by low-frequency AC electrokinetics. J. Geophys. Res. 104, 29485–29508.

Pride, S.R., 1994. Governing equations for the coupled electromagnetics and acoustics of porous media. Phys. Rev., B 50, 15678–15696.

Pride, S.R., Morgan, F.D., 1991. Electrokinetic dissipation induced by seismic waves. Geophysics 56, 914–925.

Revil, A., Leroy, P., 2001. Hydroelectric coupling in a clayey material. Geophys. Res. Lett. 28, 1643–1646.

Revil, A., Pezard, P.A., Glover, P.W.J., 1999a. Streaming potential in porous media: 1. Theory of the zeta potential. J. Geophys. Res. 104, 20021–20031.

Revil, A., Schwaeger, H., Cathles, L.M., Manhardt, P.D., 1999b. Streaming potential in porous media: 2. Theory and application to geothermal systems. J. Geophys. Res. 104, 20033–20048.

Revil, A., Hermitte, D., Voltz, M., Moussa, R., Lacas, J.-G., Bourrié, G., Trolard, F., 2002. Self-potential signals associated with variations of the hydraulic head during an infiltration experiment. Geophys. Res. Lett. 29 (7), 1106.

Revil, A., Saracco, G., Labazuy, P., 2003a. The volcano-electric effect. J. Geophys. Res. 108 (B5), 2251.

Revil, A., Naudet, V., Nouzaret, J., Pessel, M., 2003b. Principles of electrography applied to self-potential electrokinetic sources and hydrogeological applications. Water Resour. Res. 39 (5), 1114.

Sasai, Y., Shimomura, T., Hamano, Y., Utada, H., Yoshino, T., Koyama, S., Ishikawa, Y., Nakagawa, I., Yokoyama, Y., Ohno, M., Watanabe, H., Yukutake, T., Tanaka, Y., Yamamoto, T., Nakaya, K., Tsunomura, S., Muromatsu, F., Murakami, R., 1990. Volcanomagnetic effect observed during the 1986 eruption of Izu-Oshima volcano. J. Geomagn. Geoelectr. 42, 291–318.

Schaaf, A., Schmittbuhl, M., Allenbach, B., Hrehorowski, F., 1999. Four'Ellipses. Logiciel EOST, Strasbourg.

Shi, G.R., 1993. Multivariate data analysis in palaeoecology and palaeobiogeography—a review. Palaeogeogr. Palaeoclimatol. Palaeoecol. 105, 199–234.

Thouret, J.C., Finizola, A., Fornari, M., Legeley-Padovani, A., Suni, J., Frechen, M., 2001. Geology of El Misti volcano near the city of Arequipa, Peru. Geol. Soc. Am. Bull. 113 (12), 1593–1610.

Tort, A., 2003a. Morphological plasticity of the outline and the internal structures of the shell of the recent *Terebratella tenuis* sp. nov. (Brachiopoda, Terebratulida). Zoomorphology 122, 47–54.

Tort, A., 2003b. Elliptical Fourier functions as a morphological descriptor of the genus *Stenosarina* (Brachiopoda, Terebratulida, New Caledonia). Math. Geol. 35 (7), 873–885.

Viguier, B., Tort, A., 2000. Morphologie crânienne et madibulaire des Indrinae. Apports des méthodes Procrustes et des analyses de Fourier. C. R. Acad. Sci., Sci. Vie, Sér. III 323, 573–582.

Zablocki, C.J., 1976. Mapping thermal anomalies on an active volcano by the self-potential method, Kilauea, Hawaii. Proceedings, 2nd U.N. Symposium of the Development and Use of Geothermal Resources, San Francisco, California, May 1975, vol. 2, pp. 1299–1309.